Reducing the Environmental Sensitivity of Yellow Fluorescent Protein

MECHANISM AND APPLICATIONS*

Oliver Griesbeck‡§, Geoffrey S. Baird§¶, Robert E. Campbell¶, David A. Zacharias‡, and Roger Y. Tsien‡¶**

From the ‡Howard Hughes Medical Institute, ¶Department of Pharmacology, and ‖Medical Scientist Training Program and Biomedical Sciences Graduate Program, University of California, San Diego, La Jolla, California 92093-0647

Yellow mutants of the green fluorescent protein (YFP) are crucial constituents of genetically encoded indicators of signal transduction and fusions to monitor protein-protein interactions. However, previous YFPs show excessive pH sensitivity, chloride interference, poor photostability, or poor expression at 37 °C. Protein evolution in *Escherichia coli* has produced a new YFP named Citrine, in which the mutation Q69M confers a much lower pK_a (5.7) than for previous YFPs, indifference to chloride, twice the photostability of previous YFPs, and much better expression at 37 °C and in organelles. The halide resistance is explained by a 2.2-Å x-ray crystal structure of Citrine, showing that the methionine side chain fills what was once a large halide-binding cavity adjacent to the chromophore. Insertion of calmodulin within Citrine or fusion of cyan fluorescent protein, calmodulin, a calmodulin-binding peptide and Citrine has generated improved calcium indicators. These chimeras can be targeted to multiple cellular locations and have permitted the first single-cell imaging of free $[Ca^{2+}]$ in the Golgi. Citrine is superior to all previous YFPs except when pH or halide sensitivity is desired and is particularly advantageous within genetically encoded fluorescent indicators of physiological signals.

Yellow fluorescent proteins (YFPs)[1] were created (1) by mutating Thr[203] of the *Aequorea victoria* green fluorescent protein

(GFP) (2) to aromatic amino acids, typically Tyr. The resulting π-π stacking and increased local polarizability immediately adjacent to the chromophore are believed to be responsible for the ~20-nm shift to longer excitation and emission wavelengths (3). However, the changes in internal hydrogen bonding and steric packing also made the fluorescence more vulnerable to photobleaching (4, 5), decolorization by protonation (6–10), and quenching by many anions (10–12), of which chloride is the physiologically most relevant. These sensitivities can be exploited for specialized applications such as measuring fluorescence recovery after photobleaching and sensing pH and halide concentrations, but are deleterious for using YFPs either as simple fusion tags or as acceptors for fluorescence resonance energy transfer (FRET). YFPs are becoming very popular in such roles, particularly as partners for cyan fluorescent protein (CFP) mutants of GFP (2, 5, 13–15). CFPs and YFPs are spectroscopically well enough separated to be easily distinguishable in either excitation or emission spectra, yet the emission wavelengths of CFPs and excitation wavelengths of YFPs overlap well enough to make them good partners for FRET. They have largely superseded the initial pairing of blue mutants and improved green forms of GFP (16), because the blue mutants were too dim and photobleachable, and because shorter wavelengths generically excite more autofluorescence and raise more concerns of phototoxicity.

Measurements of FRET between CFP and YFP are becoming increasingly common to monitor protein-protein interactions nondestructively in live cells (5, 13, 17). The potential partners are fused to CFP and YFP, respectively, and coexpressed in cells. Because FRET requires that the CFP and YFP be within a few nanameters of each other, it can detect proximity at molecular dimensions, with 2 orders of magnitude higher spatial resolution than simple co-localization of the two colors. This approach has been used to monitor interactions of nuclear receptors and coactivators (18), nuclear transport factors (19), protein kinase A and anchoring proteins (20), G-protein subunits (21), G-protein-coupled receptors (22), and cytokine receptors (23). FRET can also detect intramolecular conformational changes, particularly within genetically encoded fluorescent indicators for a wide variety of intracellular analytes and processes such as Ca^{2+} (8, 24–26), $(Ca^{2+})_4$-CaM (27), Zn^{2+} (5), NO (28), cGMP (29, 30), protease activation (31, 32), and protein kinase A-dependent phosphorylation (33).

Genetically encoded indicators offer the major advantages of versatile and modular construction, applicability to intact transgenic organisms, and precise targetability to specific tissues, organelles, and subcellular microenvironments. These advantages are particularly important for Ca^{2+} indicators, which have been the subject of more effort than any of the other

[1] The abbreviations used are: YFP, yellow-emission variants of GFP; GFP, green fluorescent protein; CFP, cyan fluorescent protein; EYFP V68L/Q69K, GFP with mutations S65G/V68L/Q69K/S72A/T203Y; Citrine, GFP with mutations S65G/V68L/Q69M/S72A/T203Y; FRET, fluorescence resonance energy transfer; cameleon or YC, a protein construct consisting of CFP, calmodulin, M13, and YFP fused in sequence; camgaroo, a YFP with calmodulin inserted at position 145; ER, endoplasmic reticulum; PCR, polymerase chain reaction; MOPS, 4-morpholinepropanesulfonic acid; GT, galactosyltransferase.

indicator classes. Both ratiometric and non-ratiometric indicators of Ca^{2+} have been constructed from CFP, GFP, or YFP (2) as fluorophores and calmodulin as calcium binding moiety in several configurations. In cameleons (26), an N-terminal CFP is fused to calmodulin, the calmodulin-binding peptide M13 from myosin light chain kinase, and a C-terminal YFP. Binding of Ca^{2+} to calmodulin leads to a conformational change that enhances the fluorescence resonance energy transfer (FRET) from the shorter wavelength emitting CFP to the longer wavelength emitting YFP. Subsequent modifications in the YFP acceptor protein led to improved cameleons with decreased sensitivity to cytosolic pH changes (8). The YFP portion of these improved cameleons (termed EYFP V68L/Q69K) had a pK_a of 6.1, rendering it largely insensitive to pH changes near neutrality. However, due to poor folding at 37 °C, specific targeting was hard to achieve.

In a different approach, calmodulin was directly inserted into the backbone of YFP in place of Tyr^{145} to generate a medium affinity Ca^{2+} indicator termed camgaroo-1 that increased fluorescence intensity ~8-fold upon saturation with Ca^{2+} (34). A problem with this non-ratiometric indicator was that the fluorescence of the indicator in transfected cells at resting Ca^{2+} levels was almost zero, making it difficult to identify transfected cells for experiments. Also, the protein did not express well at 37 °C.

In an effort to overcome these problems, we undertook an expression screen in *Escherichia coli* and identified an improved mutant of YFP, consisting of GFP with mutations S65G/V68L/Q69M/S72A/T203Y. For brevity we have named this mutation Citrine to reflect its yellow color and acid resistance. Citrine folds well at 37 °C, can be targeted to subcellular compartments, and has a pK_a of 5.7. Some aspects of the photophysics of Citrine, including two-photon spectra, light-driven flickering, excitation state decay kinetics, and translational and rotational diffusion were recently described (35), but these measurements were wholly *in vitro*, did not document the superiority of Citrine over previous YFPs, and did not explain why the Q69M mutation conferred beneficial properties. Using Citrine, we have now constructed new genetic indicators of cellular Ca^{2+} dynamics and assessed their properties with respect to pH interference, folding, and targeting in mammalian cells. In addition, we have determined the 2.2-Å x-ray structure of Citrine and propose a structural explanation for the various improvements conferred upon Citrine by the Q69M mutation.

EXPERIMENTAL PROCEDURES

Error-prone PCR and Bacterial Colony Screening—cDNA encoding camgaroo-1 (34) in the vector pRSET$_B$ (Invitrogen) was subjected to error-prone PCR using *Taq* polymerase. The 5' primer included a *Bam*HI site and ended at the starting Met of the GFP, and the 3' primer included an *Eco*RI site and ended at the stop codon, theoretically allowing mutagenesis of every base of camgaroo-1 other than Met1. The PCR (38 cycles with annealing at 55 °C) was run in four 100-μl batches, each containing 10 μl of 10 × PCR buffer with Mg^{2+} (Roche Molecular Biochemicals), 150 μM Mn^{2+}, 250 μM of three nucleotides, 50 μM of the remaining nucleotide, and 5 ng of template. Mutagenic PCR products were combined, purified by agarose gel electrophoresis, digested with *Bam*HI and *Eco*RI, and repurified by QiaQuick columns (Qiagen). The resulting fragment was ligated into pRSET$_B$, and the crude ligation mixture was transformed into *E. coli* BL21(DE3) Gold (Stratagene) by electroporation. Bacteria plated on LB/agar plates were imaged as described (34), and colonies that became fluorescent after overnight incubation at 37 °C were grown in liquid culture and the plasmid DNA obtained by Miniprep (Qiagen). Protein was expressed and purified as previously described (34). Spectroscopy of purified protein was typically performed in 100 mM KCl, 10 mM MOPS, pH 7.25, in a fluorescence spectrometer (Fluorolog-2, Spex Industries). pH titrations were performed as described (34). All DNA sequencing was performed by the

Molecular Pathology Shared Resource, University of California, San Diego, Cancer Center.

Gene Construction and in Vitro Characterization—Mutations Q69M (Citrine), C48L, and C70V were introduced into EYFP V68L/Q69K by site-directed mutagenesis (QuikChange, Stratagene). To generate yellow cameleon-2.3 (YC2.3) and YC3.3, Citrine was inserted into the previously described cameleons YC2 and YC3 (26) in the cloning vector pUC119, and then subcloned into the mammalian expression vector pcDNA3 (Invitrogen). Targeting to the endoplasmic reticulum (ER) was achieved by the calreticulin signal peptide and the KDEL ER-retention sequence (36). Targeting to the medial/trans-Golgi was achieved using the type II membrane-anchored protein galactosyltransferase (GT), which has been used to target GFP to this organelle (6). Mitochondrial targeting of camgaroo-2 was achieved by replacing ECFP with the camgaroo-2 coding sequence in the pECFP-Mito vector (CLONTECH), which uses the targeting sequence of subunit VIII of cytochrome *c* oxidase. In order to evaluate targeted expression of YFP mutants, identical amounts of DNA (20 μg) of EYFP V68L/Q69K-ER, Citrine-ER, or Citrine C48L/C70V-ER in pcDNA3 were transfected into HeLa cells (3×10^5 per 35-mm dish) with Lipofectin (Life Technologies, Inc.). After 2 days of expression cells were suspended in Hanks' balanced saline solution, normalized at A_{600}, and measured in the fluorescence spectrometer.

Single Cell Imaging—Single HeLa cells were imaged with a charge-coupled device camera (Photometrics, Tucson, AZ) as described (26) at room temperature 1–5 days after transfection. The excitation filter for ratiometric imaging was 440DF10 with a 455DCLP dichroic mirror. The emission filters were 480DF30 (CFP) or 535DF25 (Citrine). Experiments were processed digitally using Metafluor software version 2.75 or 4.01 (Universal Imaging, West Chester, PA). For imaging camgaroo-2, a 480DF30 excitation filter was used in combination with a fluorescein dichroic mirror and emission filter 535DF25.

Crystallization and Data Collection—Citrine in vector pRSET$_B$ was expressed in *E. coli* JM109(DE3) and the protein purified as previously described (34). Following enterokinase (Invitrogen) catalyzed proteolysis of the 6-His tag, 1 ml of Ni-NTA-agarose (Qiagen) was added to bind residual uncleaved protein and 6-His peptides and the solution was gently agitated (4 °C for 2 h). Agarose resin was removed by filtration and the protein was concentrated to 20 mg/ml with a Micron-30 (Amicon). Citrine was crystallized by hanging drop vapor diffusion at 4 °C by addition of equal volumes of protein and crystallization buffer (7% PEG 3400, 50 mM NH$_4$OAc, 50 mM NaOAc, pH 5.0). Crystals were visible after 3–4 days and grew to ~$0.5 \times 0.2 \times 0.2$ mm within 14 days. The crystals belong to space group P212121 with unit cell dimensions of $a = 52.50$ Å, $b = 61.76$ Å, and $c = 70.68$ Å and one monomer per asymmetric unit. X-ray intensity data on a single crystal were collected at room temperature on a Mar 345 image plate detector (Mar Research) with a multilayer mirror monochromated CuKα beam from a Rigaku FR rotating anode x-ray generator with mirrors. The crystal diffracted to 2.2-Å resolution with an R_{merge} of 5.5 and 99.3% completeness with 4.8-fold redundancy. All data were integrated and scaled with DENZO/SCALEPACK (37). The Wilson B factor is 29.7 Å^2.

Refinement and Analysis—The atomic coordinates of the Protein Data Bank (PDB) entry 2YFP (3) with all solvent molecules, the chromophore, and residue Gln 69 removed were used as the starting model for refinement. The B factor for all atoms was set to 25 Å^2. One round of rigid body refinement, simulated annealing, and individual B factor refinement in CNS (38) resulted in an $R_{factor} = 24\%$ and an $R_{free} = 29\%$. Refinement proceeded with alternate rounds of manual adjustment in XTALVIEW (39) and simulated annealing/B factor refinement in CNS. The stereochemistry of the model was evaluated with PROCHECK (40). The most favored regions of the Ramachandran plot contained 89.6% of the nonglycine residues with the remaining 10.4% in the additional allowed regions. Cavity volumes were determined with MSMS (41).

RESULTS

Our newest and best YFP arose from efforts to improve camgaroo-1 (34), a genetically encoded Ca^{2+} indicator consisting of *Xenopus* calmodulin inserted in place of residue 145 of EYFP-Q69K (2). Camgaroo-1 had the desirable feature of a rather large (~7-fold) increase in fluorescence in response to Ca^{2+} binding, but it unfortunately expressed poorly at 37 °C and could not be targeted to organelles such as mitochondria (34). We therefore randomly mutated the cDNA encoding camgaroo-1 by error-prone PCR, transformed the resulting library into *E. coli*, and screened colonies grown at 37 °C for maximal
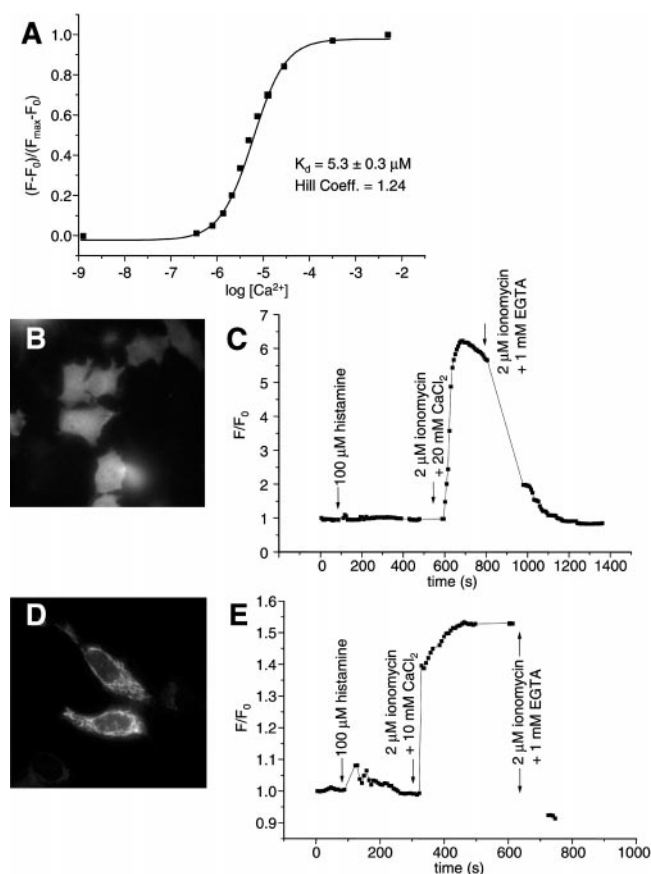
FIG. 1. **Camgaroo-2 *in vitro* and in mammalian cells.** *A,* fluorescence intensity (528 nm emission, pH 7.25) as a function of free Ca^{2+} concentrations. *B,* unstimulated HeLa cells transfected with cytosolic camgaroo-2, imaged at 480 nm excitation (30 nm band width) with a fluorescein dichroic mirror, and emission at 535 nm (25 nm band width). *C,* fluorescence changes in a HeLa cell expressing cytosolic camgaroo-2 after given stimulations. The fluorescence F normalized by the prestimulus fluorescence F_o is plotted. *D,* HeLa cells transfected with camgaroo-2 targeted to mitochondria at resting calcium levels. *E,* fluorescence changes in a HeLa cell expressing mitochondria targeted camgaroo-2 after given stimulations.

fluorescence. Sequencing of the brightest clones (camgaroo-2) revealed just one new mutation, replacement of residue 69 (Gln in wild type, Lys in EYFP V68L/Q69K) by Met. The excitation and emission maxima as well as the response to *in vitro* titration with Ca^{2+} (5.3 $\pm$ 0.3 μM apparent dissociation constant, Hill coefficient 1.24, fluorescence enhancement of ~7-fold) (Fig. 1*A*) were much the same as for camgaroo-1. However, camgaroo-2 produced far brighter expression in HeLa cells grown at 37 °C, where it filled the cytosol and nucleus uniformly (Fig. 1*B*). Stimulation of the cells with histamine produced only about 5% intensity increase (Fig. 1*C*), consistent with the bias of camgaroos toward higher amplitude $[Ca^{2+}]$ transients. A saturating elevation of cytosolic $[Ca^{2+}]$ induced with ionomycin increased the fluorescence about 6-fold (Fig. 1*C*). We also targeted camgaroo-2 to mitochondria using the pECFP-Mito vector (CLONTECH), which uses the targeting sequence of subunit VIII of cytochrome *c* oxidase. Transfected cells showed a pattern typical of mitochondria (Fig. 1*D*), indistinguishable from that of the accepted mitochondrial marker rhodamine 123 (data not shown). Camgaroo-2 is functional in mitochondria because a response to histamine was detected and ionomycin produced a significant fluorescence increase, although lower in dynamic range than in the cytosol (Fig. 1*E*).

The desirable effects of mutation Q69M in camgaroo-2 prompted transfer of this same mutation into EYFP V68L/

Q69K not containing any inserted proteins. This improved variant of YFP, *i.e.* Citrine, has excitation and emission peaks of 516 and 529 nm, respectively, a quantum yield of 0.76, and an extinction coefficient of 7.7×10^4 (Table I). These properties are comparable to those of previous YFPs. One unexpected spectroscopic difference is that Citrine photobleaches at about half the rate as EYFP V68L/Q69K (Fig. 2*A*). Based on the illumination intensity of 1.9 W/cm^2, we estimate the photobleaching quantum yield of Citrine to be about 2.3×10^{-5}, in surprisingly good agreement with an estimate of 2.6×10^{-5} obtained at much higher illumination intensities (35). The corresponding value for EYFP V68L/Q69K is 5×10^{-5} from Fig. 2*A* and Ref. 42. Citrine also has a considerably lower pK_a, 5.7, than previous YFPs such as EYFP V68L/Q69K (Fig. 2*B* and Table I) making it less sensitive to fluctuations in intracellular pH. Cytosolic pH can range from ~7.3 to 6.8, depending on cell type and stimulation (43), so cytosolic Citrine should not be expected to vary in fluorescence during normal physiological stimulation. Furthermore, pH titrations were the same in 100 mM potassium chloride and 100 mM sodium gluconate (Fig. 2*B*), indicating that Citrine is not perturbed by chloride. The pK_a values of all previous YFPs increase with increasing halide concentrations (10–12). For example, Fig. 2*B* also shows the chloride dependence of EYFP V68L/Q69K, which is actually one of the less halide-sensitive YFPs. Citrine folded efficiently at 37 °C, and with appropriate targeting sequences, could be expressed in the endoplasmic reticulum of HeLa cells. In contrast, EYFP V68L/Q69K did not tolerate attachment of ER-targeting sequences, and remained mostly nonfluorescent, with sporadic cells showing cytosolic fluorescence (data not shown). In addition, circular permutations of Citrine were observed to develop fluorescence at 37 °C (Table I), in contrast to comparable permutations of EYFP V68L/Q69K that become fluorescent only at 20 °C or less. In summary, the Q69M mutation improves many of the shortcomings of YFP including pH and chloride sensitivity as well as the inability to fold well in organelles or as a circular permutation.

To investigate why the mutation Q69M improves YFPs chloride and pH resistance, we determined the x-ray structure of Citrine at 2.2-Å resolution (Table II and PDB accession code 1HUY). As expected, the effect of the Q69M mutation on the overall structure of YFP is minor. The root mean square deviation between Citrine and the same protein with Gln at 69 (PDB accession code 1YFP) is 0.32 Å (3). In the immediate vicinity of the chromophore and the adjacent Met[69] residue, small positional shifts (on the order of 0.3 Å when compared with 1YFP) resulting from the introduction of the bulky methionine side chain are apparent (Fig. 3*A*). There is a localized slight outward displacement of the two closest strands of the β-barrel due to steric contact of the side chains of residues Val[150] and Leu[201] with the methionine. Additional residues in the local environment, including the chromophore and its π-stacked partner Tyr[203], have undergone compensatory shifts and thus the majority of the packing interactions and hydrogen bond network are unchanged.

In previous YFPs, the pK_a of the chromophore and the halide binding constant are interdependent such that protonation and halide binding facilitate each other. To explain this effect, it has been proposed that in the presence of halide, the anionic form of the chromophore is destabilized through suppressed de-localization of the negative charge (10). Conversely, neutralization of the chromophore would reduce electrostatic repulsion of an adjacent anion. Previous x-ray structural studies on YFP have shown that iodide binds in a large cavity adjacent to the chromophore and in close contact to the heterocyclic carbonyl oxygen of the chromophore (10). In the absence of halide, the

TABLE I
Spectral properties and pKa of selected YFP variants

	λ_{ex}[a]	λ_{em}[b]	ϵ[c]	Quantum yield	pK_a[d] (147 mM Cl$^-$)	pK_a[e] (no Cl$^-$)
Citrine	516	529	77×10^3	0.76	5.7	5.7
Citrine-C48L/C70V	516	529	69×10^3	0.72	5.7	ND[f]
cpCitrine[g]	506	524	20×10^3	0.10	7.7	ND
EYFP V68L/Q69K	516	529	62×10^3	0.71	6.1	6.0
cpEYFP V68L/Q69K[h]	506	524	18×10^3	0.09	8.9	ND

[a] Excitation maximum (nm).
[b] Emission maximum (nm).
[c] Extinction coefficient (M^{-1} cm^{-1}).
[d] Determined in 147 mM chloride.
[e] Determined in 147 mM gluconate.
[f] ND, not determined.
[g] Circularly permuted Citrine.
[h] Circularly permuted EYFP V68L/Q69K.

FIG. 2. **Photobleaching and pH/Cl$^-$ dependence of Citrine *versus* EYFP V68L/Q69K.** *A,* photobleaching curves for microdroplets of EYFP V68L/Q69K or Citrine under oil, observed on a fluorescence microscope with 1.9 W/cm^2 centered at 490 nm. Time constants for single or double-exponential fits to the bleaching curves are listed. *B,* pH dependence of the fluorescence (at 528 nm) of Citrine in the presence (○) or absence (×) of 100 mM Cl$^-$, and likewise of EYFP V68L/Q69K (■, ◆).

TABLE II
Data collection and refinement statistics

Data collection	
Resolution (Å)[a]	28.3–2.2 (2.28–2.20)
No. of reflections[a]	12106 (1181)
Completeness (%)[a]	99.3 (99.7)
R_{merge} (%)[a,b]	5.5 (14.4)
Refinement Statistics	
R_{cryst} (%)[a]	16.4 (19.5)
R_{free} (%)[a,c]	20.8 (26.0)
No. of solvent molecules	97
Average B factor (Å^2)	
Main chain	26.3
Side chain	29.4
Solvent	35.5
Stereochemistry	
Root mean square deviation bond length (Å)	0.009
Root mean square deviation bond angle (°)	1.3

[a] Numbers in parentheses refer to the highest resolution shell.
[b] $R_{merge} = \Sigma|I_{hkl} - I_{av}|/\Sigma I_{av}$.
[c] R_{free} was calculated using about 10% of the reflections which were omitted from the refinement.

conformational change was permitted, it is unlikely that the thioether side chain of Met could contribute to the formation of a halide-binding site since it is incapable of hydrogen bonding in the same manner as the carboxamide nitrogen of a Gln side chain. The benefits of Q69M are not generalizable across GFP colors, because this mutation prevents CFPs from becoming fluorescent (results not shown). CFPs have bulkier chromophores based on Trp rather than Tyr at position 66, so their intolerance of increased adjacent bulk at position 69 is not surprising.

We wondered whether removal of the two cysteines in GFPs could further improve folding in the oxidative environment of the secretory pathway. For this purpose we introduced the mutations C48L and C70V into GFP mutants. These mutations had previously been found to be the least injurious replacements for the cysteines in GFP itself.[2] When introduced into CFP or EYFP V68L/Q69K, these mutants retained fluorescence but became extremely temperature-sensitive and developed bright fluorescence only after overnight growth at 4 °C or room temperature. Cysteine-less Citrine was brightly fluorescent, folded well at 37 °C, and had spectroscopic properties similar to Citrine itself, with only a slight decrease in quantum yield and extinction coefficient (Table I). However, in HeLa cells, ER-targeted cysteine-less Citrine gave less fluorescence intensity and lower expression than ER-targeted Citrine containing cysteines, as verified by Western blot analysis. Therefore, the cysteines were left in Citrine for all subsequent constructs for either cytosolic or targeted expression.

We then set out to construct a series of improved genetic

binding cavity (55 Å^3) is partially occupied by the side chain of Gln[69] (Fig. 3*B*). In order to form the anion binding cavity, the side chain of this residue must undergo a conformational change and swing out of the cavity thereby expanding the cavity size (91 Å^3) and positioning the nitrogen of the carboxamide such that it can hydrogen bond to the anion (Fig. 3*C*). In Citrine, Gln[69] has been replaced with a Met that effectively fills the halide-binding cavity such that it is no longer accessible to a sphere with radius 1.2 Å (Fig. 3*A*). In the x-ray structure of Citrine, the Met is well ordered (B_{av} = 17.5 Å^3) and there is no unexplained difference density in the region of the cavity. This suggests that the Met side chain is tightly packed into the cavity and likely unable to undergo a conformational change that would be analogous to that observed for Gln[69] between the free and iodide bound forms of EYFP (10). Even if such a
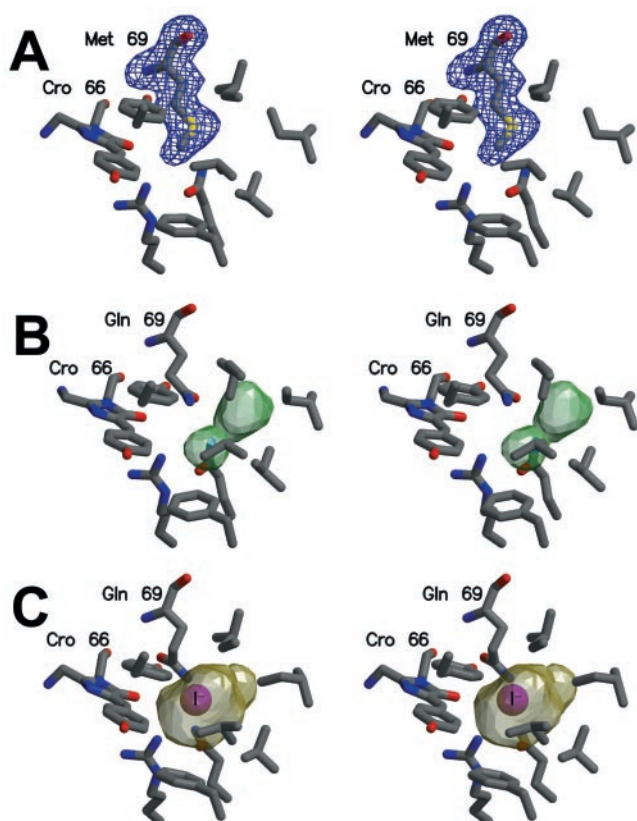
FIG. 3. **Detailed view of residue 69 and surrounding residues from the x-ray structures of Citrine, EYFP-H148G (PDB accession code 1F0B), and EYFP-H148G with bound iodide (PDB accession code 1F09).** *A,* stereoview of residue Q69M of Citrine with the chromophore (*Cro 66*) and surrounding residues (Arg[96], Val[150], Ile[152], Val[163], Phe[165], Gln[183], Leu[201], and Tyr[203]). The electron density represents a $F_o - F_c$ omit map contoured at 3σ calculated with the final refined coordinates in which the occupancy of Gln[69] was set to zero. *B,* the *apo* form of EYFP-H148G (10) in the same orientation as *A* with the cavity (55 Å[3]) is shown in *green*. The cavity represents the volume accessible to a sphere of probe radius 1.2 Å. *C.* The iodide bound form of EYFP-H148G (10) with the iodide ion represented as a *purple sphere* that is not meant to represent its van der Waals radius. The total volume (91 Å[3]) of the halide-binding cavity is represented in *yellow*. The programs CNS (38), MSMS (41), CONSCRIPT (50), and MOLSCRIPT (51) were used to construct this figure.

FIG. 4. **Dependence of YC3.3 fluorescence on Ca²⁺ and pH *in vitro.*** *A,* emission spectrum of YC3.3 in the presence of 100 μM EGTA (*solid line,* −Ca²⁺) or 100 μM CaCl₂ (*dotted line,* +Ca²⁺) at pH 7.25. Excitation was at 432 nm. *B,* emission ratio of YC3.3 (528/476 nm) in the presence of 100 μM CaCl₂ (■) or 100 μM EGTA (●) were measured at the given pH values. Corresponding ratios for YC2.1 (8) in 100 μM CaCl₂ (□) or 100 μM EGTA (○) are shown for comparison.

indicators that incorporated Citrine in place of previous YFPs. Yellow cameleons YC2.3 and YC3.3 are new ratiometric indicators of high and medium calcium affinity based on previous cameleons (8, 26), but incorporating Citrine as the FRET acceptor protein. The spectral changes in the emission of purified YC3.3 from 100 μM EGTA to calcium saturation were as expected (Fig. 4*A*), indicating that substitution of EYFP V68L/Q69K with Citrine did not alter the Ca²⁺-dependent FRET changes. The ratio of 528/476 nm emissions was stable down to approximately pH 6.5, and then decreased with further acidification (Fig. 4*B*). The pH effects were greatest at saturating Ca²⁺, at which FRET from the relatively pH-insensitive CFP to the still somewhat pH-sensitive Citrine is maximal. Nevertheless YC2.3 and 3.3 are more resistant than any other cameleon to acidic pH. YC2.3 and YC3.3 were brightly fluorescent when expressed in the cytosol of HeLa cells and were homogenously distributed in the cytosol with the nucleus excluded, as expected of a 74-kDa protein without targeting sequences. Responses to submaximal doses of histamine were readily detected, and the maximal ratio change obtained in cells was around 2-fold (data not shown), similar to the results from previous cameleons (8).

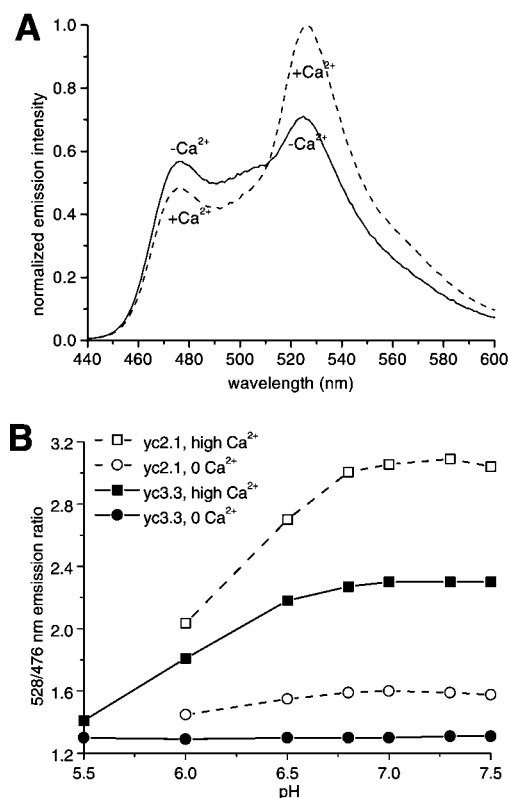The lower pK_a of Citrine compared with previous YFPs

should allow imaging of free calcium transients in more acidic compartments that so far have been inaccessible to cameleons. For example, the Golgi was reported to have a pH of 6.58 (6), which should still be in the working range of our new cameleons. To test this we targeted YC3.3 to the Golgi by fusing the 81 N-terminal amino acids of human galactosyltransferase type II to YC3.3 and thereby generating GT-YC3.3 (Fig. 5*A*). Transfection of HeLa cells resulted in bright punctate labeling of Golgi stacks in a juxtanuclear position (Fig. 5*B*), identical to cells transfected with GT-EYFP or stained for the medial/trans-Golgi marker α-mannosidase II (6). GT-YC3.3 was saturated at resting conditions (Fig. 5*C*), indicating a high concentration of free Ca²⁺ in the Golgi. Histamine (100 μM) caused a very small decrease. The Golgi calcium store could be depleted with several washes of ionomycin/EGTA and was refilled upon readmitting extracellular calcium (Fig. 5*C*), demonstrating the feasibility of single cell imaging of free calcium concentrations in the Golgi of mammalian cells. It has to be kept in mind that ionomycin does not perform optimally in acidic compartments. Also it should be noted that YC3.3 is near its lower pH limit under these conditions. Further improvements in pH resistance are still desirable, especially if one wants to study even more acidic compartments of interest such as secretory vesicles. YC3.3 was similarly well expressed in the ER (data not shown).

DISCUSSION

Citrine represents a third generation of YFPs or yellow mutants of green fluorescent protein. The first generation was exemplified by S65G/S72A/T203Y (26) and "10C" (1), S65G/V68L/S72A/T203Y. These proteins proved to be quite sensitive to pH (*e.g.* pK_a 6.9–7.1) (6), halides such as Cl⁻ (11) and
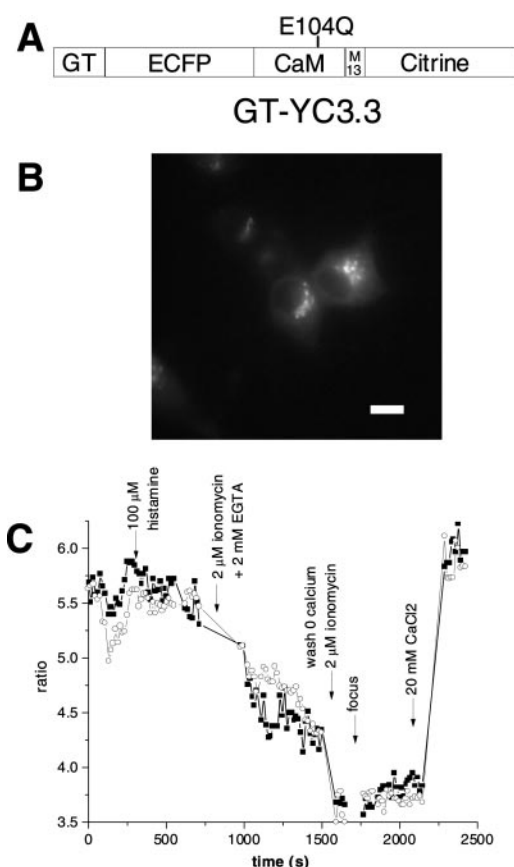
FIG. 5. **Calcium measurements with improved cameleons targeted to the Golgi of HeLa cells.** *A,* schematic structure of GT-YC3.3. *GT*, 81 N-terminal amino acids of human galactosyltransferase type II. *CaM*, calmodulin. The E104Q substitution within calmodulin raises the apparent dissociation constant for Ca^{2+} to 1.5 μM (8). *B,* HeLa cells transfected with GT-YC3.3. Excitation was at 440 nm (10-nm band width), the dichroic mirror transition was at 455 nm, and emission was collected at 535 nm (25 nm band width). *Scale bar,* 10 μM. *C,* emission ratios of two HeLa cells expressing GT-YC3.3 after stimulations with agonists. CFP emission was collected at 480 nm (30-nm band width) with excitation and YFP emission as described in *B.*

partially reversible photobleaching (4). These sensitivities have been useful for particular purposes such as quantifying cytosolic pH (6), $[Cl^-]$ (12, 44), or FRET efficiency (18), but are considerable nuisances whenever one simply wants to use YFP as a reliable label or FRET acceptor. In a second generation, the mutation Q69K was introduced into 10C to give S65G/V68L/Q69K/S72A/T203Y (8) or "EYFP V68L/Q69K," which lowered the pK_a to 6.1 with little effect on the other sensitivities. We speculated that the positively charged lysine might electrostatically hinder chromophore protonation (8). The Q69K mutation also introduced a disadvantage: folding became noticeably more difficult, especially in organelles at 37 °C. In the most recent version, Citrine, replacement of Q69K by Q69M lowered the pK_a yet further to 5.7, eliminated the halide sensitivity, doubled the photostability, and improved the folding. The improvement in folding efficiency was particularly apparent in difficult cases such as functional expression at 37 °C in organelles or with an internally inserted calmodulin, *i.e.* camgaroo-2. The crystal structure provides some reasonable rationalizations for these improved properties, in that the Met side chain nicely plugs what had been a sizable halide-binding cavity next to the chromophore. The poorer folding of Q69K might well be due to the extra length of a Lys side chain making an uncomfortable fit within the cavity, or the electrostatic penalty for burying a positive charge, or both. Thus a good steric fit with a neutral side chain seems far more effective

at lowering the chromophore pK_a than an awkward fit with a positively charged side chain. The apparent photobleaching of YFPs probably consists of two components, a reversible proton redistribution or tautomerization and a truly irreversible covalent reaction (4, 5). Either or both would be hindered by better packing of the hydrophobic core and elimination of a cavity next to the chromophore.

Despite the inferiority of Q69K, it was an essential stepping stone in the evolution of better properties by random mutagenesis and screening, because direct alteration of the Gln codon CAG to the Met codon ATG would require two base changes in a single codon, a very unlikely event. It was fortunate that there was an easy evolutionary path from CAG to the Lys codon AAG and then to ATG. Many other examples of optimal sequences may remain relatively inaccessible to random mutation due to barriers created by the genetic code.

We have demonstrated the application of Citrine in a series of genetically encoded Ca^{2+} indicators based on Citrine, all of which were improved in relation to their predecessors. Camgaroo-2 may constitute an alternative to cameleons in confocal microscopy given that it can be conveniently excited at the 488 nm argon laser line, or in cases in which targeting of cameleons are not successful. For example, we and others have found targeting of cameleons to mitochondria to be difficult (45), whereas camgaroo-2 was easy to send to the mitochondria with the targeting sequence of cytochrome *c* oxidase subunit VIII. Single cell imaging of mitochondrial calcium offers exciting new prospects for studying its dynamics in this organelle as well as to address aspects of heterogeneity of the mitochondrial population (46). Camgaroos lack a CaM-binding peptide and therefore have lower Ca^{2+} affinities than the newest generic design of GFP-based Ca^{2+} indicators, "G-CaMP" (47) or "pericams" (45). These indicators are chimeras of the CaM-binding peptide M13, circularly permuted GFP or YFP, and CaM. However, many of these molecules still do not express well at 37 °C, so annealing mutations corresponding to Q69M might well be worth incorporating.

Our new improved cameleons expressed well at 37 °C and were successfully targeted to the ER and Golgi. Cytosolic pH fluctuations are readily transmitted to the ER (48), therefore it was important to be able to express a pH-resistant functional indicator in this organelle, which had not been possible with previous versions of cameleons. Similarly, previous cameleons did not allow imaging free calcium in the Golgi due to the mild acidity of the compartment, which quenched other YFPs. Little is known about calcium regulation in the Golgi. One study using targeted aequorin identified the Golgi as a major calcium store within the cell (49), but aequorin has many disadvantages, such as lack of intrinsic fluorescence and requirement for an exogenous cofactor, that limit its use as a reliable calcium probe. We believe that Citrine should supersede previous YFPs within fusions for multicolor observation of protein trafficking, protein-protein interaction, and intramolecular conformational change, especially within genetically encoded Ca^{2+} indicators.

REFERENCES

1. Ormö, M., Cubitt, A. B., Kallio, K., Gross, L. A., Tsien, R. Y., and Remington, S. J. (1996) *Science* **273,** 1392–1395
2. Tsien, R. Y. (1998) *Annu. Rev. Biochem.* **67,** 509–544
3. Wachter, R. M., Elsliger, M.-A., Kallio, K., Hanson, G. T., and Remington, S. J. (1998) *Structure* **6,** 1267–1277
4. Dickson, R. M., Cubitt, A. B., Tsien, R. Y., and Moerner, W. E. (1997) *Nature* **388,** 355–358
5. Miyawaki, A., and Tsien, R. Y. (2000) *Methods Enzymol.* **327,** 472–500
6. Llopis, J., McCaffery, J. M., Miyawaki, A., Farquhar, M. G., and Tsien, R. Y. (1998) *Proc. Natl. Acad. Sci. U. S. A.* **95,** 6803–6808
7. Matsuyama, S., Llopis, J., Deveraux, Q. L., Tsien, R. Y., and Reed, J. C. (2000) *Nat. Cell Biol.* **2,** 318–325

8. Miyawaki, A., Griesbeck, O., Heim, R., and Tsien, R. Y. (1999) *Proc. Natl. Acad. Sci. U. S. A.* **96,** 2135–2140
9. Elsliger, M.-A., Wachter, R. M., Hanson, G. T., Kallio, K., and Remington, S. J. (1999) *Biochemistry* **38,** 5296–5301
10. Wachter, R. M., Yarbrough, D., Kallio, K., and Remington, S. J. (2000) *J. Mol. Biol.* **301,** 157–171
11. Wachter, R. M., and Remington, S. J. (1999) *Curr. Biol.* **9,** R628–R629
12. Jayaraman, S., Haggie, P., Wachter, R. M., Remington, S. J., and Verkman, A. S. (2000) *J. Biol. Chem.* **275,** 6047–6050
13. Tsien, R. Y., and Miyawaki, A. (1998) *Science* **280,** 1954–1955
14. Ellenberg, J., Lippincott-Schwartz, J., and Presley, J. F. (1999) *Trends Cell Biol.* **9,** 52–56
15. Green, G., Kain, S. R., and Angres, B. (2000) *Methods Enzymol.* **327,** 89–94
16. Heim, R., and Tsien, R. Y. (1996) *Curr. Biol.* **6,** 178–182
17. Zacharias, D. A., Baird, G. S., and Tsien, R. Y. (2000) *Curr. Opin. Neurobiol.* **10,** 416–421
18. Llopis, J., Westin, S., Ricote, M., Wang, J., Cho, C. Y., Kurokawa, R., Rose, D. W., Rosenfeld, M. G., Tsien, R. Y., and Glass, C. K. (2000) *Proc. Natl. Acad. Sci. U. S. A.* **97,** 4363–4368
19. Damelin, M., and Silver, P. A. (2000) *Mol. Cell* **5,** 133–140
20. Ruehr, M. L., Zakhary, D. R., Damron, D. S., and Bond, M. (1999) *J. Biol. Chem.* **274,** 33092–33096
21. Janetopoulos, C., Jin, T., and Devreotes, P. (2001) *Science* **291,** 2408–2411
22. Overton, M. C., and Blumer, K. J. (2000) *Curr. Biol.* **10,** 341–344
23. Siegel, R. M., Frederiksen, J. K., Zacharias, D. A., Chan, F. K. M., Johnson, M., Lynch, D., Tsien, R. Y., and Lenardo, M. J. (2000) *Science* **288,** 2354–2357
24. Romoser, V. A., Hinkle, P. M., and Persechini, A. (1997) *J. Biol. Chem.* **272,** 13270–13274
25. Persechini, A., Lynch, J. A., and Romoser, V. A. (1997) *Cell Calcium* **22,** 209–216
26. Miyawaki, A., Llopis, J., Heim, R., McCaffery, J. M., Adams, J. A., Ikura, M., and Tsien, R. Y. (1997) *Nature* **388,** 882–887
27. Persechini, A., and Cronk, B. (1999) *J. Biol. Chem.* **274,** 6827–6830
28. Pearce, L. L., Gandley, R. E., Han, W., Wasserloos, K., Stitt, M., Kanai, A. J., McLaughlin, M. K., Pitt, B. R., and Levitan, E. S. (2000) *Proc. Natl. Acad. Sci. U. S. A.* **97,** 477–482
29. Sato, M., Hida, N., Ozawa, T., and Umezawa, Y. (2000) *Anal. Chem.* **72,** 5918–5924
30. Honda, A., Adams, S. R., Sawyer, C. L., Lev-Ram, V., Tsien, R. Y., and Dostmann, W. R. G. (2001) *Proc. Natl. Acad. Sci. U. S. A.* **98,** 2437–2442
31. Mahajan, N. P., Harrison-Shostak, D. C., Michaux, J., and Herman, B. (1999) *Chem. Biol.* **6,** 401–409
32. Vanderklish, P. W., Krushel, L. A., Holst, B. H., Gaily, J. A., Crossin, K. L., and Edelman, G. M. (2000) *Proc. Natl. Acad. Sci. U. S. A.* **97,** 2253–2258
33. Nagai, Y., Miyazaki, M., Aoki, R., Zama, T., Inouye, S., Hirose, K., Iino, M., and Hagiwara, M. (2000) *Nat. Biotechnol.* **18,** 313–316
34. Baird, G. S., Zacharias, D. A., and Tsien, R. Y. (1999) *Proc. Natl. Acad. Sci. U. S. A.* **96,** 11241–11246
35. Heikal, A. A., Hess, S. T., Baird, G. S., Tsien, R. Y., and Webb, W. W. (2000) *Proc. Natl. Acad. Sci. U. S. A.* **97,** 11996–12001
36. Kendall, J. M., Dormer, R. L., and Campbell, A. K. (1992) *Biochem. Biophys. Res. Comm.* **189,** 1008–1016
37. Otwinowski, Z., and Minor, W. (1997) *Methods Enzymol.* **276,** 307–326
38. Brunger, A. T., Adams, P. D., Clore, G. M., DeLano, W. L., Gros, P., Grosse-Kunstleve, R. W., Jiang, J. S., Kuszewski, J., Nilges, M., Pannu, N. S., Read, R. J., Rice, L. M., Simonson, T., and Warren, G. L. (1998) *Acta Cryst. D Biol. Cryst.* **54,** 905–921
39. McRee, D. E. (1999) *J. Struct. Biol.* **125,** 156–165
40. Laskowski, R. A., MacArthur, M. W., Moss, D. S., and Thornton, J. M. (1993) *J. Appl. Cryst.* **26,** 283–291
41. Sanner, M. F., Olson, A. J., and Spehner, J. C. (1996) *Biopolymers* **38,** 305–320
42. Baird, G. S., Zacharias, D. A., and Tsien, R. Y. (2000) *Proc. Natl. Acad. Sci. U. S. A.* **97,** 11984–11989
43. Chesler, M., and Kaila, K. (1992) *Trends Neurosci.* **15,** 396–402
44. Kuner, T., and Augustine, G. J. (2000) *Neuron* **27,** 447–459
45. Nagai, T., Sawano, A., Park, E., and Miyawaki, A. (2001) *Proc. Natl. Acad. Sci. U. S. A.* **98,** 3197–3202
46. Rizzuto, R., Pinton, P., Carrington, W., Fay, F. S., Fogarty, K. E., Lifshitz, L. M., Tuft, R. A., and Pozzan, T. (1998) *Science* **280,** 1763–1766
47. Nakai, J., Ohkura, M., and Imoto, K. (2001) *Nat. Biotechnol.* **19,** 137–141
48. Kim, J. H., Johannes, L., Goud, B., Antony, C., Lingwood, C. A., Daneman, R., and Grinstein, S. (1998) *Proc. Natl. Acad. Sci. U. S. A.* **95,** 2997–3002
49. Pinton, P., Pozzan, T., and Rizzuto, R. (1998) *EMBO J.* **17,** 5298–5308
50. Lawrence, M. C., and Bourke, P. D. (2000) *J. Appl. Cryst.* **33,** 990–991
51. Kraulis, P. J. (1991) *J. Appl. Cryst.* **24,** 946–950